Available online at www.sciencedirect.com

ScienceDirect

Current Opinion in
Colloid & Interface Science

Forced flows in liquid bridges

Ilia V. Roisman[1], Mohammad Abboud[1], Philipp Brockmann[1], Fiona Berner[2], Rüdiger Berger[2], Pauline Rothmann-Brumm[3], Hans Martin Sauer[3], Edgar Dörsam[3] and Jeanette Hussong[1]

Abstract

Wetting of solid surfaces by liquid deposition, contact dispensing, drop transfer, collision of wet particles, or during coating processes is often accompanied by the formation of liquid bridges between two or more solid substrates. They appear in many applications, like material science, microfluidics, biomedical, chemical, or aerospace engineering, and different fields of physics. In this study, the flows accompanying lifting of a Hele-Shaw cell, stretching or shearing of a liquid bridge, as well as liquid bridge flows observed during printing processes and other important applications, are briefly reviewed. Such flows are governed by surface tension, inertia, stresses associated with the liquid rheology, and forces caused by the substrate's wettability. Instabilities of liquid bridges lead to the formation of finger-like structures on the substrate or the appearance of cavities at the wetted region of the wall. The time required for jet pinch-off also determines the residual liquid volume on both solid bodies.

Addresses

[1] Institute for Fluid Mechanics and Aerodynamics, Technische Universität Darmstadt, Alarich-Weiss-Straße 10, 64287 Darmstadt, Germany

[2] Max Planck Institute for Polymer Research, Ackermannweg 10, 55128 Mainz, Germany

[3] Institute of Printing Science and Technology, Technische Universität Darmstadt, Magdalenenstraße 2, 64289 Darmstadt, Germany

Corresponding author: Roisman, Ilia V. (roisman@sla.tu-darmstadt.de)

Current Opinion in Colloid & Interface Science 2023, **67**:101738

This review comes from a themed issue on **Wetting and Spreading (2023)**

Edited by **Tatiana Gambaryan-Roisman** and **Victor Starov**

For complete overview about the section, refer Wetting and Spreading (2023)

https://doi.org/10.1016/j.cocis.2023.101738

Keywords

Liquid bridge, Coating, Jet breakup, Interfacial instability, Cavitation, Dewetting.

Introduction

A liquid bridge is a small volume of liquid that connects two solid surfaces or objects. It forms due to the surface tension of the liquid, which causes it to adopt a curved shape between the two surfaces [1,2]. The stability of the liquid bridge depends on the size of the liquid volume, the surface properties of the objects, and the surrounding environment.

In many cases, liquid bridges are formed by stretching a liquid volume that initially wets a finite area between two bodies. Stretchable liquid bridges have numerous applications in different fields. The list of these applications[1] includes:

- Material Science: The behavior of liquid bridges under stretching can be studied to understand the properties of materials such as adhesion, surface tension, and rheology [3]. This knowledge can be used to develop new materials with improved properties.
- Microfluidics: Stretching liquid bridges are used in microfluidic devices to manipulate small volumes of fluids [4–6]. This is particularly useful in biological applications such as cell culture and drug delivery.
- Biomedical Engineering: Stretching liquid bridges are used in tissue engineering to mimic the mechanical forces experienced by living tissues [7,8]. This can help in the development of better artificial tissues and organs.
- Chemical Engineering: The behavior of liquid bridges can be used to optimize industrial processes such as coating, painting, and printing. This can lead to improved product quality and reduced manufacturing costs.
- Physics: Stretching liquid bridges are used as model systems to study fundamental physics concepts such as fluid mechanics, interfacial phenomena, and nonlinear dynamics [9,10]. Among the phenomena that are studied using liquid bridges are Marangoni or buoyancy convection, flows accompanied by melting,

[1] As an experiment, this list of current applications of liquid bridges has been initially prepared with the help of artificial intelligence (AI) chatbot *chatGPT*, which provided a surprisingly useful text. The text created by an AI algorithm has been accepted and further edited by the human authors.

boiling, solidification, or crystallization, and many others.

- Aerospace Engineering: Liquid bridges are used in the design and testing of microgravity propulsion systems [11–14]. In these systems, liquid bridges can be used to control the flow of propellant in a microgravity environment where traditional pumps and valves do not work. Another application of liquid bridges in aerospace engineering is in the development of cooling systems for spacecraft. Liquid bridges can be used to transport heat away from sensitive electronic components in a microgravity environment [15], where traditional cooling systems are not effective.

Typical forced flow configurations in liquid bridges include stretching, shear deformations, flows in open channels, or flows in the meniscus in the contact region of two rolling cylinders, as schematically shown in Figure 1. The latest achievements in the study of the dynamics and instabilities of liquid bridges in these four main configurations will be briefly reviewed in this article.

Dynamics and instability of stretching liquid bridges

Many physical processes are significantly influenced by the dynamics of stretching liquid bridges, shown schematically in Figure 1a, or can be associated with such flows. One example is the interaction of an impacting particle with a wet substrate or the collision of wet solid particles. In Ref. [16] the restitution coefficient of an impacted particle has been measured and modeled for different volumes of the liquid bridge. Oblique and normal impacts of a solid particle onto a wet substrate have been studied in Refs. [17,18] and modeled, considering the effect of stretching of the liquid bridge formed between the substrate and the particle during rebound. A theoretical model of the collision of several wet particles [19], which accounts for inertial, viscous, and capillary effects in a stretching liquid bridge, is able to predict the outcome of the collision: rebound, agglomeration, or even a Newton's cradle, which can happen for three particles. Such studies are very important for better understanding and reliable modeling of particle agglomeration, wet particle fluidization [20], ice crystal ice accretion [21], or the material properties of wet granular media [22].

Dynamics of stretching of Newtonian bridges

The simplest case of the stretching of a liquid Newtonian bridge between two plates, one of which moves, is illustrated in Figure 2. The phenomena include the flow in a thin gap between two separating plates (lifted Hele-Shaw cell), the formation of a stretching ligament between two menisci, and its breakup.

Viscous flow in a thin gap (lifted Hele-Shaw cell)

The process of liquid bridge stretching starts with the flow in a thin gap between the plates, as shown in Figure 2a. If the radius $R(t)$ of the liquid spot is much larger than the gap height $H(t)$ and if the inertial effects in the flow are negligibly small in comparison to the viscous stresses, the axisymmetric flow in the gap far from the meniscus is described by a solution [23] of Landau and Lifshitz (1959)

$$v_r = 3\dot{H}\frac{rz(z-H)}{H^3}, \quad v_z = \dot{H}\left(\frac{3z^2}{H^2} - \frac{2z^3}{H^3}\right), \qquad (1)$$

where v_r and v_z are the radial and axial components of the velocity relative to the fixed plate, z-axis is directed in the direction of the moving plate. The expression for the

Figure 1

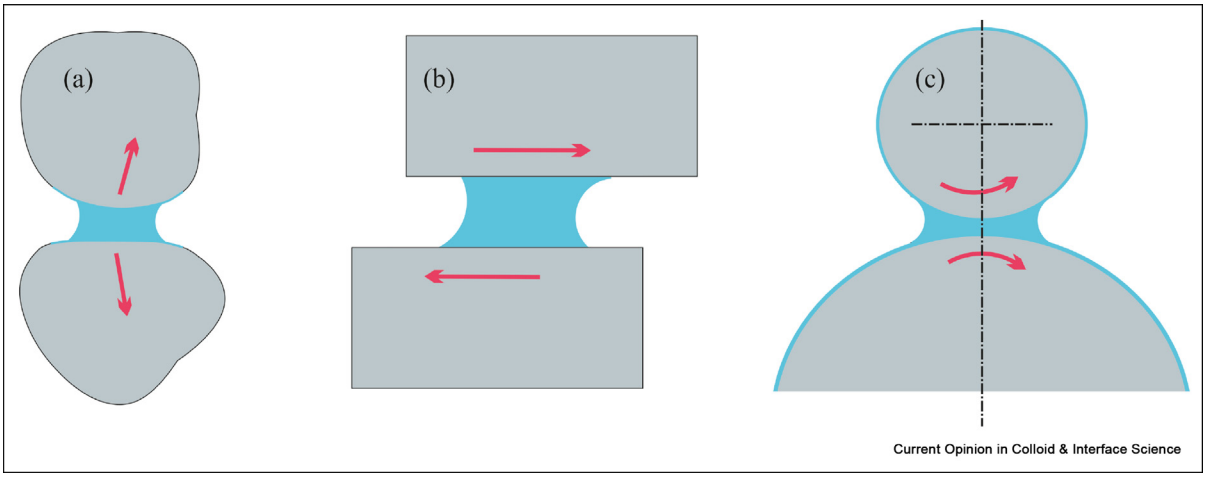

Selected examples of forced flows in liquid bridges are: (**a**) liquid bridge stretching; (**b**) shear deformation; and (**c**) the flow associated with the rolling motion of cylinders.

Figure 2

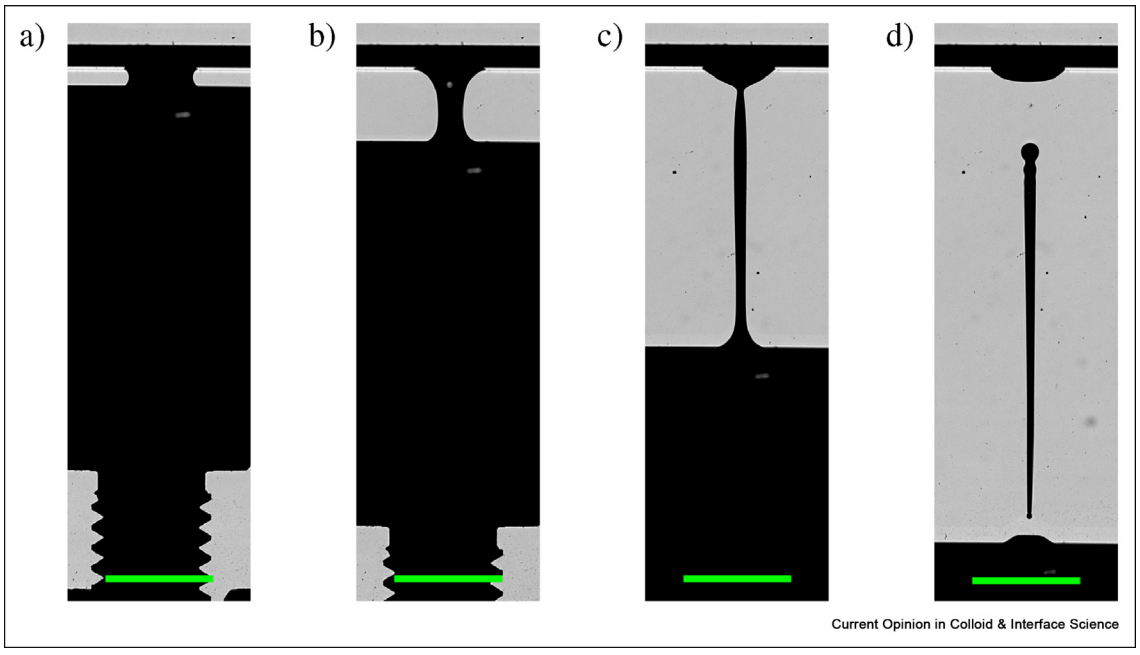

Fast stretching of a Newtonian liquid bridge between two parallel plates. The lower plate moves with a constant acceleration of a = 150 ms^{-2}. The initial droplet volume is 5 μl with an initial plate separation of H = 1.03 mm. The length of the scale bar is 10 mm. The Liquid is a mixture of 26.46 wt% water, 32.30 wt% glycerin, and 41.24 wt% ammonium thiocyanate with a dynamic viscosity of μ_{RIM} = 4.99 cPa. The main stages include: (**a**) flow in a thin gap between plates; (**b**) formation of a jet, connecting two menisci; (**c**) jet stretching; and (**d**) pinch-off.

pressure in the gap, accounting for the pressure jump at the moving meniscus, is

$$p \approx \frac{3\mu \dot{H}}{H^3}\left(r^2 - R^2\right) - \sigma\left(\frac{2}{H} + \frac{1}{R}\right), \tag{2}$$

where μ and σ are the liquid viscosity and surface tension.

Finally, the mass balance of an axisymmetric incompressible flow in the gap yields.

$$\dot{R}(t) = \frac{R\dot{H}}{2H}. \tag{3}$$

This simple, basic solution is not valid for all the parameters. The mass balance is not precise since, at high rates of stretching, the plates are wetted by a thin residual liquid layer [24], although the observations show that the meniscus apparently recedes.

The evolution of the radius of the liquid bridge (3) is valid only for cases where the cross-section is circular and uniform. This is not always the case since if the initial gap between the plates is small enough, the flow becomes unstable. Various types of outcomes of liquid bridge stretching are shown in Figure 3. They include fingering instability, cavitation phenomena leading to the nucleation and expansion of lacunas in the liquid at the substrate interface, and the emergence of dendrite-like or tree-like structures.

The formation of these fingers at the liquid interface is often related to the Saffman–Taylor instability, which corresponds to the liquid flowing in a porous medium. In fact, the dynamics leading to the fingering instability in the stretching layer in a thin gap are much more similar to the Rayleigh–Taylor instability, which is caused by a positive pressure gradient at the interface. It can be shown that the typical distance l_{fingers} between fingers is scaled well as

$$l_{\text{fingers}} \sim \sqrt{\frac{\sigma}{p_{,n}}}, \tag{4}$$

where the pressure gradient in the axisymmetric case is $p_{,n} = \partial p/\partial r$. For the Rayleigh–Taylor instability caused by gravity, the value of the pressure gradient is ρg, and for the interface acceleration, it is ρa.

The main dimensionless numbers governing the fingering instability of Newtonian liquid bridges include the geometrical parameter λ and the capillary number Ca, defined as

Figure 3

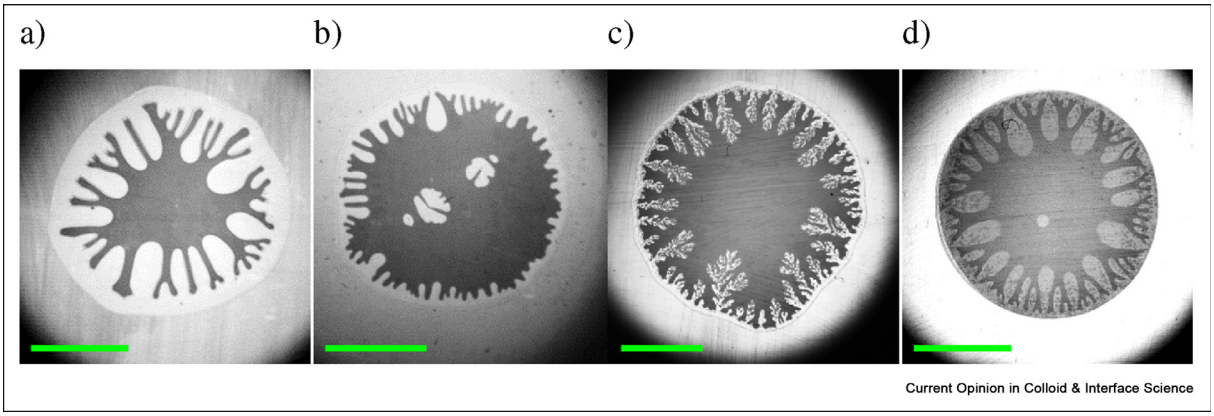

Various outcomes of a liquid bridge stretching in a thin gap between parallel plates. Lifted Hele-Shaw cell with a constant acceleration $a = 5$ m/s^2. Liquids used in a–c) are a mixture of 26.46 wt% water, 32.30 wt% glycerin, and 41.24 wt% ammonium thiocyanate with a dynamic viscosity of $\mu_{RIM} = 4.99$ cPa, while in d) it is a diluted ink dye. The length of the scale bar is 5 mm. **a**) Fingering, pure liquid, $H_0 = 46$ μm, $R_0 = 6.10$ mm; **b**) fingering and cavitation, pure liquid, $H_0 = 38$ μm, $R_0 = 5.91$ mm; **c**) fingering in a suspension, 30 μm particles, $H_0 = 57$ μm, $R_0 = 7.32$ mm; **d**) fingering and cavitation in a diluted ink dye of shear thinning rheology, $H_0 = 40$ μm, $R_0 = 5.78$ mm.

$$\lambda = \frac{H_0}{2R_0}, \quad Ca = \frac{a^{1/2}R_0\mu}{\sqrt{2H_0}\sigma}, \tag{5}$$

However, also the Reynolds number $\mathrm{Re} = \rho a^{1/2}H_0^{3/2}/\mu$ can influence the outcome if its value is significant.

The fingering instability is analyzed in an experimental and theoretical study [25] for a liquid bridge stretched with constant acceleration. The model is able to predict the maximum number of fingers and the threshold conditions for the appearance of fingers.

In the experimental study [26], various mesh-like structured liquid films have been obtained in a lifted Hele-Shaw cell, while one of the plates is porous. The effect of a bubble on fingering instability is investigated in a purely theoretical study [27]. Here, the results of the linear stability analysis are compared with the full-scale computational fluid dynamics (CFD) computations.

In [28], the case of a liquid drop squeezing and stretching between two plates under the action of a constant force is studied. They have shown that the evolution of the bridge radius follows the $R \sim t^{1/8}$ relation, which can be demonstrated using force balance and the known expression (2) for the pressure in the axisymmetric case. However, in this study, the analysis is focused on complex non-axisymmetric cases, which include non-symmetric fingering instability, expansion and merging of several bridges, and the effect of bubble expansion.

Stretching of a liquid jet and breakup

As soon as the distance between the separating plates becomes much longer than the wetting diameter of the bridge, a stretching liquid jet is formed between the two menisci. The mass and axial momentum balance in a long, nearly circular jet is usually expressed in the form [29].

$$\frac{\partial f}{\partial t} + \frac{\partial uf}{\partial z} = 0, \quad \frac{\partial uf}{\partial t} + \frac{\partial u^2 f}{\partial z} = \frac{1}{\rho}\frac{\partial F}{\partial z}, \tag{6}$$

where u is the axial velocity of the liquid in the jet, z is the axial coordinate, $f(z, t) \equiv \pi R^2$ is the area of the jet cross-section, and F is the total stretching force applied to the jet cross-section, which accounts for the capillary pressure in the jet, surface tension, and the internal stresses associated with the jet rheology. For Newtonian liquids, the expression for the force yields:

$$F = 3\mu f\frac{\partial u}{\partial z} + \pi\sigma R\left[K + K^3 R\frac{\partial^2 R}{\partial z^2}\right], \quad K = \left[\left(\frac{\partial R}{\partial z}\right)^2 + 1\right]^{-1/2}. \tag{7}$$

Such a quasi one-dimensional model has been applied [30] for the description of the jet drawn out of a bath of a viscous Newtonian liquid, accounting also for gravity effects. The evolution of the ligament shape and the breakup height are predicted by the model. In Ref. [31] the breakup of an electrically induced liquid bridge of nearly conical shape has been studied. Two main breakup mechanisms are identified and modeled; spontaneous and stretching breakups.

Liquid bridge breakup at fast bridge stretching between two plates, one of which moves with a constant acceleration, has been studied in Ref. [32]. At high plate acceleration, its velocity at some instant exceeds the typical capillary velocity along the bridge, $V \sim \sqrt{\sigma/\rho R}$. The outcome of the bridge stretching at such accelerations does not depend on the plate's acceleration.

The flow regime in the liquid bridge at long times is determined by the Reynolds number and Weber number

$$\mathrm{Re} = \frac{\rho a^{1/2} R_0 H_0^{1/2}}{\mu}, \quad We = \frac{\rho a R_0 H_0}{\sigma}, \tag{8}$$

respectively. The Reynolds number determines the threshold distance between plates at which the viscous and inertial stresses are comparable. The Weber number determines the distance at which the jet starts to stretch freely due to inertia.

Two main time scales are introduced, the characteristic capillary time t_σ and the viscous time scale t_μ, defined as

$$t_\sigma = \sqrt{\frac{\rho R_0^3}{\sigma}}, \quad t_\mu = \left[\frac{\mu^2 \rho R_0^5}{\sigma^3}\right]^{1/4}. \tag{9}$$

The viscous time is associated with the instant when the viscous part of the force applied to the ligament cross-section is equal to the capillary force. It is shown that the pinch-off time of the stretching bridge scales well with t_σ in low-viscosity liquids, for which the Reynolds number is much higher than unity. For low Reynolds numbers, the breakup time is well scaled by the viscous time t_μ.

Rheologically complex, non-Newtonian liquid bridges

Complex fluids are heterogeneous mixtures that exhibit non-Newtonian behavior due to the coexistence of two or more phases, such as solid-liquid suspensions, granular solids, foams, and emulsions. The mechanical properties of complex fluids are governed by the interplay of various physical forces and length scales, including intermolecular interactions, particle-particle interactions, and phase separation [33]. Consequently, these fluids display a rich variety of mechanical responses, including solid-like elasticity, fluid-like flow, and viscoelastic behavior. Therefore, most industrial liquids are complex liquids, and their extensional rheology is relevant to various industrial applications. In polymer processing, the stretching and elongation of polymer melts during manufacturing can lead to defects that affect the mechanical and physical properties of the final product, rendering understanding the uniaxial and biaxial stretching of polymer melts critical for producing high-quality polymer products [34]. In the food industry, extensional rheology is crucial for understanding the sensory properties of complex fluids like mayonnaise, yogurt, and other similar products [35]. The extensional behavior of these fluids affects their texture and mouthfeel, which are important factors in determining consumer acceptance. Additionally, extensional rheology has applications in other fields, such as biotechnology, where it can be used to study the behavior of complex biological fluids under stress, such as blood clots [36]. Other applications worth mentioning, including but not limited to, are fiber spinning, film blowing, blow molding, thermoforming, wire coating, and foaming [3].

For Newtonian liquids, the extensional viscosity is 3 times their shear viscosity, as can be found in the expression (7), while for complex liquids this ratio varies. The ratio between extensional viscosity and dynamic viscosity is known as the Trouton Ratio ($\mathrm{Tr} = \eta_e/\eta_s$).

Furthermore, the behavior of a fluid under fast extension depends on the relationship between the strain rate and the fluid's relaxation time. This correlation is referred to as the Deborah number (De) ($De = \dot{\epsilon}_0 \lambda$), which is the ratio of the characteristic response time of the fluid to the characteristic flow time. Viscoelastic fluids have a De between 0.5 and 10, while a $\mathrm{De} \ll 1$ means that the fluid will be predominantly viscous, and a $\mathrm{De} \gg 10$ indicates an elastic fluid with behavior similar to a Hookian spring. The Weissenberg number (Wi), on the other hand, compares elastic forces to viscous forces regardless of the time frame considered.

Near the moment of pinch-off, the nonlinear dynamics undergo a significant transformation owing to the pronounced effects of additional elastic stresses and non-Newtonian shear and extensional viscosities [37]. The necking of a viscous liquid has been described in a well-known theoretical study [38]. The typical shapes of the jets before pinch-off; however, are significantly influenced by the liquid rheology. A detailed overview of such shapes for different models of non-Newtonian liquids can be found in Ref. [39].

Flows of suspensions

It is well known that the effective viscosity of a suspension increases with increasing local particle volume fractions. Shear-induced or inertial particle migration in the flow of a suspension can result in the local accumulation of particles and hence local variations in the effective viscosity. While particle migration might occur even at low volume fractions, at higher particle volume fractions, shear thinning [40], shear thickening [41,42] and jamming can lead to dramatic changes in the effective viscosity [43–45]. Jamming of particles means that a collection of particles becomes "stuck" in a

particular configuration, forming a rigid structure [44,46–48]. Given that, it can easily be expected that the bridge stretching behavior gets more complex depending on the dynamics of the process and the amount and type of particles involved.

The behavior of liquid bridges can be significantly affected by the presence of suspended particles in the liquid. Even at low solid volume fractions of about 1–3%, where the volume fraction does not affect the viscosity, particles can induce disturbances that lead to an accelerated thinning and breakup of the bridge [49].

In general, when a liquid bridge containing particles is stretched, particles can form local agglomerations of particles, which lead to the formation of sharp local contractions, and voids of particles, which rapidly break down and lead to an accelerated breakup compared to a pure liquid [43,50,51], as schematically shown in Figure 4a and b.

Thereby, in the course of the process, the effect of particles on the dynamics varies. In the beginning, the dynamics can be described by the effective viscosity of the suspension [52,57]. This regime is followed by a second regime, determined by the properties of the interstitial fluid, corresponding to a fluid without particles [54,57]. In this regime, which occurs when the neck diameter reaches the particle length scale, the presence of the grains in the neck prevents the formation of a long, stable filament, leading to very localized thinning, resulting in an accelerated breakup compared to the pure liquid [54], as shown schematically in Figure 4. Larger Particles were found to result in an earlier breakup than smaller particles [57]. The crossover between the regimes was described as a function of grain size and initial volume fraction [54].

Figure 4

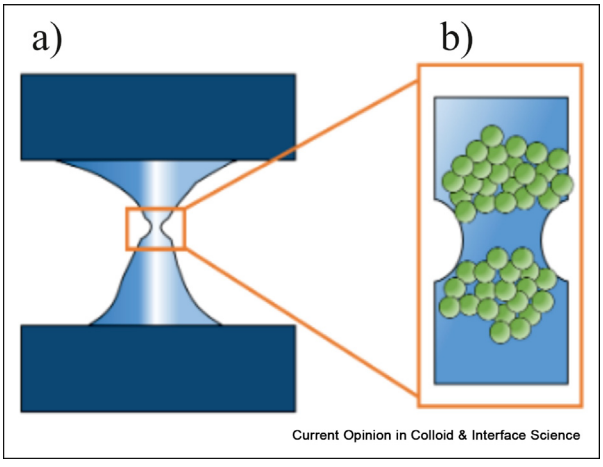

Sketch of the necking phenomenon in stretched suspensions, inspired by the observations [52–56]. **a**) Necking in a dense suspension in liquid bridge stretching; **b**) formation of particle clusters during necking.

At high shear rates and high volume fractions, jamming might occur in the liquid bridge, leading to its abrupt breakup [43]. Thereby, the strain rate required for jamming-induced breakup varies by orders of magnitude if Φ is varied between 0.58 and 0.62 [43].

The presence of solid particles can enhance interfacial instabilities [58–61]. In the case of a suspension in a lifted Hele-Shaw cell, the instabilities can lead to the emergence of fingers and dendrite-like structures, as shown in examples in Figure 3c. The mechanism responsible for particle-induced fingering is attributed to the accumulation of particles at the fluid-fluid interface (meniscus), resulting in a gradient of effective viscosity that induces miscible fingering [58,59].

Recently, polydisperse suspensions and suspensions with non-Newtonian fluids have become the subject of research [62–64]. In a viscoelastic suspension, the initial neck formation and blistering instability are affected by the presence of particles [62]. A recent study shows that the difference in pinch-off time compared to a pure liquid decreases linearly with increasing amounts of small particles in bidisperse suspensions [63].

Friction forces on shear driven bridges

A better understanding of shearing flows in liquid bridges is necessary for the modeling of wet granular media [65,66] or for the characterization of the wetting properties of solid substrates. These flows are determined by the capillary forces in the liquid bridge and by the forces associated with the substrate's wettability and morphology [67].

Classically, the wetting properties of surfaces are characterized by contact angle measurements, namely the determination of the advancing contact angle θ_a and the retracting contact angle θ_r. However, the forces associated with the wetting or dewetting of surfaces also depend on the microscopic disturbances of the contact line caused by local contamination or local abrasion of the surface. Therefore, it is particularly important to understand what additional forces are caused by local variations in wetting properties.

The lateral force F_{lateral} applied to a liquid bridge or to a liquid drop sliding on a flat substrate is [68].

$$F_{\text{lateral}} = k\sigma w(\cos\theta_r - \cos\theta_a) \tag{10}$$

where w is the width of the wet spot, σ is the surface tension of the liquid, and $k \approx 1$ is a dimensionless factor determined by the shape of the contact line [69]. This expression is valid only in cases where the capillary number,

based on the propagation velocity, is much smaller than unity and the variation of the contact angle with the propagation velocity can be neglected. On a perfectly smooth and uniform substrate, the value of the k number is equal to unity. The measured value of k on real surfaces can thus be used as an additional characteristic value associated with the density of local surface disturbances.

A device [71] for direct measurement of the force F_{lateral}, a drop friction force instrument (DoFFI), is based on the method presented initially by Hitoshi and Suda in 2003 [72]. This method has been used by various research groups for the characterization of surfaces [73–75].

In DoFFI, a droplet sticks to a force sensor by capillary action. A stable liquid bridge forms between the end of the force sensor and the surface (Figure 5a). A ring holder is used to better control the near-spherical shape of the bridge. When the sample moves laterally, the force sensor deflects, and the droplet deforms until θ_a and θ_r are reached. Then the droplet starts sliding over the surface. Typically, drop volumes of microliters, i.e., drop diameters of millimeters, exhibit friction forces in the micro-Newton regime, depending on the nature of the liquid and the surface.

The ring-holder influences the geometry of a liquid bridge (Figure 5b – inset) and thus the value of the measured force F_{lateral}, as shown in Figure 5b, while the values of θ_a and θ_r remain constant [70].

Moreover, a sessile drop requires a higher force to initiate movement (depinning force) than to maintain movement [76]. The magnitude of this depinning force is proportional to the size of the surface defects [77]. This result agrees well with the theoretical predictions by Joanny and de Gennes published in the 1980s [78].

Moreover, a sessile drop requires a higher force to initiate movement than to maintain movement on any solid surface with contact angle hysteresis [76]. The magnitude of this depinning force is proportional to the size of the surface defects [77]. This result agrees well with the theoretical predictions by Joanny and de Gennes published in the 1980s [78] and droplet evaporation studies [79].

Recently, the DoFFI device has been extended into a 2D characterization tool named scanning DoFFI [70]. This tool allows one to determine wetting maps of surface samples having sizes of several square centimeters and to resolve wetting features from centimeter to submillimeter sizes (Figure 5c).

Another surface force apparatus has been developed in Ref. [80] and used for measurements of the lateral and normal forces applied to a liquid bridge between two parallel plates. They have developed a simplified model that allows them to predict these forces. A more sophisticated theoretical model for the shear force, which accounts for the complex geometry of liquid bridges on rough substrates, can be found in Ref. [81]. Earlier [82], we presented a force apparatus that allows decoupling normal and lateral adhesion forces acting on the drop by adding a tilted stage to a rotary stage.

Liquid bridge dynamics during printing processes and other applications

A comprehensive review on of dynamics of liquid bridges in cases relevant to printing can be found in Ref. [83]. Liquid bridges appear in various types of printing presses at the instant of ink splitting. Several examples are shown in Figure 6. In rotary printing techniques such as gravure, flexography, or offset

Figure 5

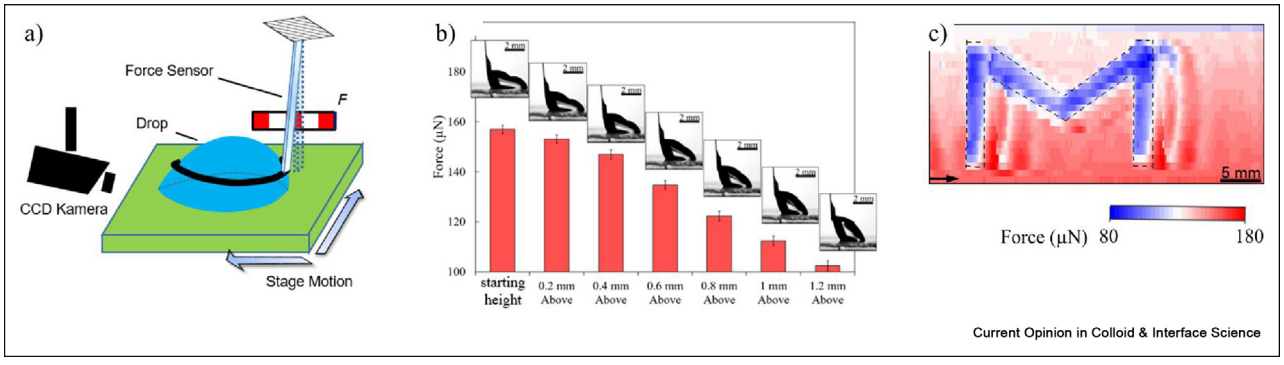

Liquid drop sliding between a moving plate and a solid drop holder, connected to a force sensor. **a**) Schematic view of the ring-shaped drop holder. The bending of the glass micropipette is read-out with a CCD video camera; **b**) dependence of the friction force on the distance of the ring relative to the surface; **c**) wetting map of a structured substrate obtained using a sDoFFI device. The surface consists of an M-shaped structure with high (outside the "M") and low contact angle hysteresis (inside the "M"). Adopted from Ref. [70].

Figure 6

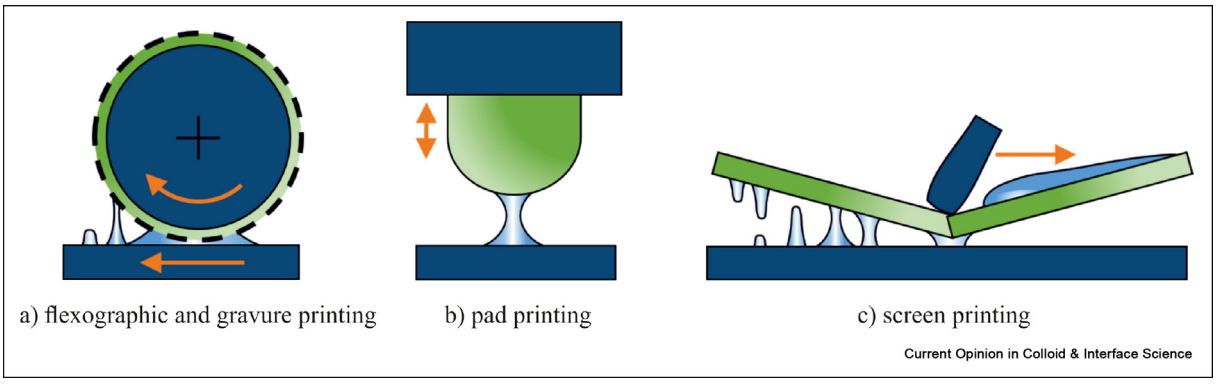

Schematic overview of liquid bridges in printing technologies: **a**) flexographic and gravure printing; **b**) pad printing; and **c**) screen printing.

lithography, shown schematically in Figure 6a; see Ref. [83], the printed image is represented by a raster or pattern of small sessile ink drops of a few tens of micrometers in size, which are transferred from the printing cylinder to the substrate in a rolling motion. The velocity v_p of printing may range over three orders of magnitude, from a few cm/s in, e.g., pad printing, to 15 m/s in the fastest rotogravure and flexographic web-fed presses. At the moment when the surfaces of the printing cylinder are lifted from the substrate, the foot points of the ink drops are mutually retracted with an acceleration of $a = v_p^2/R$, where R is the radius of the cylinder, creating liquid filaments and sheets that last for a few milliseconds.

In pad printing (see Figure 6b), ink is transferred by a stamping motion from a flat gravure plate with tiny cells filled with ink to the substrate by use of a soft, hyperelastic silicone pad [84]. Liquid bridges form on two subsequent occasions: when the pad is lifted from the plate and when it is lifted from the substrate after it has deposited the ink there. In screen printing, the ink is pressed through the tiny pores, i.e., typically 10−100 μm in size, in an elastic printing mesh kept under tension. Ink squeeze is accomplished by means of an elastic blade or squeegee pressed on the rear side of the mesh. The mesh comes into contact with the substrate under the tip of the blade. When the blade is then pulled across the mesh, as in Figure 6c, ink passes through the pores [85]. Ink splitting takes place at each point of the substrate when the blade tip has passed and the mesh is released from the surface.

In advance of splitting, rotary printing presses force the ink through a microscopically small gap between the cylinder and substrate. One may therefore distinguish an early and a late regime [86] of ink splitting in the nip. The early phase is characterized by a shear flow of the ink, creating a negative pressure that destabilizes the ink meniscus on the diverging side of the nip [87]. Shear rates of the order of 10^6 s^{-1} and velocities v_p of several m/s are typical. The numbers $Ca = \eta v_p/\sigma$ are of order of 10^{-3}−10 only, and the Laplace and Reynolds numbers are small because of the very narrow gap width of 0.1−1 μm. Contrastingly, the late phase of ink splitting is essentially of the elongation type, with progressive thinning and breakdown of the liquid bridges in the nip [88]. Laplace numbers are of the order of 100, which is accompanied by vigorous drop formation, or *fogging*. One finds linear filaments as well as liquid sheets, and actually, high-speed video records show the expected capillary waves [86].

The question of the mechanism thatdetermines the volume of these bridges arises. Commonly, one assigns liquid bridge size to the Saffman−Taylor instability [89]. However, recent high-speed video visualizations [90] show that liquid bridge formation in the gravure printing nip has a much more complex phenomenology. The wedge between the cylinder and the substrate develops to a steady state in which an excess volume of ink is constantly conducted in the nip in addition to the ink in the gravure cells. This excess volume depends on both v_p and cell volume, a phenomenon that has no counterpart in the Hele-Shaw cell. The excess volume creates a closed ink meniscus in the wedge between the cylinder and substrate, which is the origin of the viscous fingering pattern. Liquid bridges seeded from here have a typical length scale of 150−300 μm.

Scaling laws of finger size with capillary number may therefore differ from the $Ca^{-1/2}$-behavior observed in the Hele-Shaw cell [91]. Scaling exponents are shifted when elastic surfaces [92] or shear-thinning inks are used [93,94], or when the cell filling process by the doctor blade is dependent on v_p by itself [87]. A key study on these effects of finger size selection is *Carvalho & Scriven* [95]. Interestingly, the scaling exponent they

obtained is close to −0.9. This is not only far from the Saffman−Taylor result but also from most printing experiments. Values between −0.3 and −0.5 are common here. We believe that this discrepancy results is another effect of the varying excess volume in the nip and that the instability is actually a higher-order one, as in the Hele-Shaw cell.

Unresolved problems and critical issues

Major challenges in the future research of liquid bridges are associated with:

- Rheologically complex or multiphase liquids, liquids with surfactants, especially accounting for the complexity of modeling their wetting properties.
- Rough, morphologically, or chemically structured substrates.
- Flows with phase change, like freezing or boiling.
- Unstable, relatively fast realistic flows accompany modern technological processes like printing or coating.

Let us revisit the topic of fingering during gravure printing discussed in §4. With onset of the finger formation, ink may float forth and back through the nip and couple the meniscus to the delicate equilibrium of viscous shear forces in the nip. To the knowledge of the authors, this is unique within the family of hydrodynamic instabilities, and the linear stability analysis in Ref. [95] is incomplete. One of the perspectives here could be the data-driven recognition of the principal degrees of freedom and the governing equations of pattern formation [96−98]. This is a challenging task because of the huge quantities of experimental data needed, but could be accomplished with the aid of machine-learning-assisted pattern recognition, applied to, e.g., video records of liquid bridge dynamics in the gravure nip [90] or viscous fingering scans from mass production on industrial-scale printing presses [91,99]. Adequate software tools have proven their versatility [100]. It is crucial to realize that viscous fingering in the nip cannot be assigned to only one specific type of hydrodynamic instability but comprises transitions between different non-linear, stochastic systems [87], an insight that is not new in relation to liquid bridges [101]. This can give rise to beautiful, highly symmetric ornament patterns [91] as well as those resembling more irregular vascular networks [102].

Declaration of generative AI and AI-assisted technologies in the writing process

During the preparation of this work the authors used *chatGPT* in order to list all existing fields of application for liquid bridges. After using this tool/service, the authors reviewed and edited the content as needed and take full responsibility for the content of the publication.

Declaration of competing interest

The authors declare the following financial interests/personal relationships which may be considered as potential competing interests:
Ilia Roisman reports financial support and article publishing charges were provided by German Research Foundation. Edgar Dörsam reports financial support was provided by German Research Foundation. Ruediger Berger reports financial support was provided by German Research Foundation. Jeanette Hussong reports financial support was provided by German Research Foundation. Ilia Roisman reports financial support was provided by European Union. Ilia Roisman is husband of Tatiana Gambaryan-Roisman, who is a co-editor of the special issue.

Data availability

No data was used for the research described in the article.

Acknowledgments

This research was supported by the German Scientific Foundation (Deutsche Forschungsgemeinschaft) in the framework of the SFB-1194 Collaborative Research Center "Interaction between Transport and Wetting Processes" (No 265191195), projects A03, C01 and C07N. This project has received funding from the European Union's Horizon 2020 research and innovation program under the Marie Skłodowska-Curie grant agreement No 955612 (NanoPaInt). The authors would like to thank the support of SFB-1194 for providing open access to this publication.

References

Papers of particular interest, published within the period of review, have been highlighted as:

* of special interest
** of outstanding interest

1. Plateau J: **The figures of equilibrium of a liquid mass**. *Annu Rep Smithson Inst* 1864:338−369.
2. Orr F, Scriven L, Rivas AP: **Pendular rings between solids: meniscus properties and capillary force**. *J Fluid Mech* 1975, **67**:723−742.
3. McKinley GH, Sridhar T: **Filament-stretching rheometry of complex fluids**. *Annu Rev Fluid Mech* 2002, **34**:375−415.
4. Marston PL, Thiessen DB: **Manipulation of fluid objects with acoustic radiation pressure**. *Ann N Y Acad Sci* 2004, **1027**: 414−434.
5. Feng J, Song Q, Zhang B, Wu Y, Wang T, Jiang L: **Large-scale, long-range-ordered patterning of nanocrystals via capillary-bridge manipulation**. *Adv Mater* 2017, **29**:1703143.
6. Wu L, Dong Z, Li F, Song Y: **Designing laplace pressure pattern for microdroplet manipulation**. *Langmuir* 2018, **34**:639−645.
7. Wang L, Qiu M, Yang Q, Li Y, Huang G, Lin M, *et al.*: **Fabrication of microscale hydrogels with tailored microstructures based on liquid bridge phenomenon**. *ACS Appl Mater Interfaces* 2015, **7**:11134−11140.
8. Ehrig S, Schamberger B, Bidan CM, West A, Jacobi C, Lam K, *et al.*: **Surface tension determines tissue shape and growth kinetics**. *Sci Adv* 2019, **5**, eaav9394.
9. Sakata T, Terasaki S, Saito H, Fujimoto S, Ueno I, Yano T, *et al.*: **Coherent structures of m= 1 by low-Stokes-number particles suspended in a half-zone liquid bridge of high aspect ratio: microgravity and terrestrial experiments**. *Physical Review Fluids* 2022, **7**:14005.

10. Šeta B, Dubert D, Massons J, Gavalda J, Bou-Ali MM, Ruiz X: **Effect of Marangoni induced instabilities on a melting bridge under microgravity conditions**. *Int J Heat Mass Tran* 2021, **179**:121665.

11. Weislogel MM, Graf J, Wollman AP, Turner C, Cardin K, Torres L, *et al.*: **How advances in low-g plumbing enable space exploration**. *npj Microgravity* 2022, **8**:16.

12. Li JC, Lin H, Li K, Zhao JF, Hu WR: **Liquid sloshing in partially filled capsule storage tank undergoing gravity reduction to low/micro-gravity condition**. *Microgravity Sci Technol* 2020, **32**: 587–596.

13. Chen S, Duan L, Kang Q: **Study on propellant management device in plate surface tension tanks**. *Acta Mech Sin* 2021, **37**: 1498–1508.

14. Nijhuis J, Schmidt S, Tran NN, Hessel V: **Microfluidics and macrofluidics in space: ISS-proven fluidic transport and handling concepts**. *Front Space Technol* 2022, **2**:16.

15. Kang Q, Wu D, Duan L, Hu L, Wang J, Zhang P, *et al.*: **The effects of geometry and heating rate on thermocapillary convection in the liquid bridge**. *J Fluid Mech* 2019, **881**:951–982.

16. * Grohn P, Oesau T, Heinrich S, Antonyuk S: **Investigation of the influence of impact velocity and liquid bridge volume on the maximum liquid bridge length**. *Adv Powder Technol* 2022, **33**: 103630.
This is a further study of this group on impact of a solid particle onto a wetted substrate. Better understanding of the dynamics of a liquid bridge allows to improve the modeling of particle agglomeration and accretion.

17. Ma J, Liu D, Chen X: **Normal and oblique impacts between smooth spheres and liquid layers: liquid bridge and restitution coefficient**. *Powder Technol* 2016, **301**:747–759.

18. Buck B, Tang Y, Deen NG, Kuipers J, Heinrich S: **Dynamics of wet particle–wall collisions: influence of wetting condition**. *Chem Eng Res Des* 2018, **135**:21–29.

19. Davis RH: **Simultaneous and sequential collisions of three wetted spheres**. *J Fluid Mech* 2019, **881**:983–1009.

20. Xu H, Wang W, Ma C, Zhong W, Yu A: **Recent advances in studies of wet particle fluidization characteristics**. *Powder Technol* 2022:117805.

21. Currie T, Struk P, Tsao JC, Fuleki D, Knezevici D: **Fundamental study of mixed-phase icing with application to ice crystal accretion in aircraft jet engines**. In *4th AIAA atmospheric and space environments conference*; 2012:3035.

22. Nowak S, Samadani A, Kudrolli A: **Maximum angle of stability of a wet granular pile**. *Nat Phys* 2005, **1**:50–52.

23. Landau LD, Lifshitz EM: *Fluid mechanics*. New York: Pergamon Press; 1959 [transl. J. B. Sykes & W. H. Reid].

24. Brulin S: *Hydrodynamic investigations of rapidly stretched liquid bridges* [Phd thesis]. Darmstadt, Germany: Technische Universität Darmstadt.; 2021.

25. Brulin S, Roisman IV, Tropea C: **Fingering instability of a viscous liquid bridge stretched by an accelerating substrate**. *J Fluid Mech* 2020, **899**:A1.

26. Kanhurkar SD, Gandhi PS, Bhattacharya A: **Evolution of mesh-like liquid films in multi-port lifted Hele Shaw cells**. *Chem Eng Sci* 2022, **252**:117499.

27. Kanhurkar SD, Patankar V, ul Islam T, Gandhi PS, Bhattacharya A: **Stability of viscous fingering in lifted Hele-Shaw cells with a hole**. *Phys Rev Fluids* 2019, **4**:94003.

28. ** Moffatt H, Guest H, Huppert HE: **Spreading or contraction of viscous drops between plates: single, multiple or annular drops**. *J Fluid Mech* 2021, **925**:A26.
Theoretical and experimental study on deformation of a liquid bridge between plates, description of the radius evolution, fingering instability in non axisymmetric cases, including multiple bridges and bubbles.

29. Yarin AL: *Free liquid jets and films: hydrodynamics and rheology*. New York: Longman Publishing Group; 1993.

30. ** Wei X, Rivero-Rodríguez J, Zou J, Scheid B: **Statics and dynamics of a viscous ligament drawn out of a pure-liquid bath**. *J Fluid Mech* 2021, **922**:A14.
Theoretical model for the description of a Newtonian ligament drawn out of a liquid bath. The evolution of the ligament shape and the breakup height are predicted by the model.

31. Xu XY, Xu Z, Wang XD, Wang LD, Qin SC, Liu JS, *et al.*: **Breakup mechanism of the electrically induced conical liquid bridge**. *Phys Fluids* 2022, **34**:52118.

32. Brulin S, Tropea C, Roisman IV: **Pinch-off of a viscous liquid bridge stretched with high Reynolds numbers**. *Colloids Surf A Physicochem Eng Asp* 2020, **587**:124271.

33. Chhabra RP: **Non-Newtonian fluids: an introduction**. *Rheol Complex Fluids* 2010:3–34.

34. * Münstedt H: **Extensional rheology and processing of polymeric materials**. *Int Polym Process* 2018, **33**:594–618.
This paper summarizes the most recent nodels for extensional rheology of polymers and their related lab experiments. It gives an interesting perspective on the applicability of lab stretching rheological data in various industrial polymer processes such as spinning, thermoforming, drawing, casting, blowing, bubble stability, and foaming.

35. Ahmed J, Ptaszek P, Basu S: **Food rheology: scientific development and importance to food industry**. In *Advances in food rheology and its applications*. Elsevier; 2017:1–4.

36. Sousa PC, Vaz R, Cerejo A, Oliveira MS, Alves MA, Pinho FT: **Rheological behavior of human blood in uniaxial extensional flow**. *J Rheol* 2018, **62**:447–456.

37. Dinic J, Jimenez LN, Sharma V: **Pinch-off dynamics and dripping-onto-substrate (DoS) rheometry of complex fluids**. *Lab Chip* 2017, **17**:460–473.

38. Eggers J: **Universal pinching of 3D axisymmetric free-surface flow**. *Phys Rev Lett* 1993, **71**:3458.

39. ** Hassager O, Wang Y, Huang Q: **Extensional rheometry of model liquids: simulations of filament stretching**. *Phys Fluids* 2021, **33**:123108.
detailed overview of the predicted shapes of stretching jets for different models of non-Newtonian liquids.

40. Chatté G, Comtet J, Nigues A, Bocquet L, Siria A, Ducouret G, *et al.*: **Shear thinning in non-Brownian suspensions**. *Soft Matter* 2018, **14**:879–893.

41. Stickel J, Powell R: **Fluid mechanics and rheology of dense suspensions**. *Annu Rev Fluid Mech* 2005, **37**:129–149.

42. Morris JF: **Shear thickening of concentrated suspensions: recent developments and relation to other phenomena**. *Annu Rev Fluid Mech* 2020, **52**:121–144.

43. Smith M, Besseling R, Cates M, Bertola V: **Dilatancy in the flow and fracture of stretched colloidal suspensions**. *Nat Commun* 2010, **1**:114.

44. Mewis J, Wagner NJ: *Colloidal suspension rheology*. Cambridge University Press; 2012.

45. Abbas M, Magaud P, Gao Y, Geoffroy S: **Migration of finite sized particles in a laminar square channel flow from low to high Reynolds numbers**. *Phys Fluids* 2014, **26**:123301.

46. Bertrand E, Bibette J, Schmitt V: **From shear thickening to shear-induced jamming**. *Phys Rev E* 2002, **66**:60401.

47. Lootens D, Van Damme H, Hébraud P: **Giant stress fluctuations at the jamming transition**. *Phys Rev Lett* 2003, **90**:178301.

48. Singh A, Ness C, Seto R, de Pablo JJ, Jaeger HM: **Shear thickening and jamming of dense suspensions: the "roll" of friction**. *Phys Rev Lett* 2020, **124**:248005.

49. Lindner A, Fiscina JE, Wagner C: **Single particles accelerate final stages of capillary break-up**. *Europhys Lett* 2015, **110**: 64002.

50. Zhao H, Liu HF, Xu JL, Li WF, Lin KF: **Inhomogeneity in breakup of suspensions**. *Phys Fluids* 2015, **27**:63303.

51. Mathues W, McIlroy C, Harlen OG, Clasen C: **Capillary breakup of suspensions near pinch-off**. *Phys Fluids* 2015, **27**:93301.

52. Furbank RJ, Morris JF: **Pendant drop thread dynamics of particle-laden liquids**. *Int J Multiphas Flow* 2007, **33**:448–468.

53. Alexandrou AN, Bazilevskii A, Entov V, Rozhkov A, Sharaf A: **Breakup of a capillary bridge of suspensions**. *Fluid Dyn* 2010, **45**:952–964.

54. Bonnoit C, Bertrand T, Clément E, Lindner A: **Accelerated drop detachment in granular suspensions**. *Phys Fluids* 2012, **24**: 43304.

55. Moon JY, Lee SJ, Ahn KH, Lee SJ: **Filament thinning of silicone oil/poly (methyl methacrylate) suspensions under extensional flow**. *Rheol Acta* 2015, **54**:705–714.

56. Connington KW, Miskin MZ, Lee T, Jaeger HM, Morris JF: **Lattice Boltzmann simulations of particle-laden liquid bridges: effects of volume fraction and wettability**. *Int J Multiphas Flow* 2015, **76**:32–46.

57. ** Château J, Guazzelli É, Lhuissier H: **Pinch-off of a viscous suspension thread**. *J Fluid Mech* 2018, **852**:178–198.
Provides a comprehensive analysis of the two regimes that occur during the detachment of a droplet's liquid bridge, with a particular focus on a wide range of particle sizes and volume fractions at large Ohnesorge numbers. This study identifies unifying scaling for these regimes, offering valuable insights into this complex phenomenon.

58. Tang H, Grivas W, Homentcovschi D, Geer J, Singler T: **Stability considerations associated with the meniscoid particle band at advancing interfaces in Hele-Shaw suspension flows**. *Phys Rev Lett* 2000, **85**:2112.

59. Xu F, Kim J, Lee S: **Particle-induced viscous fingering**. *J Non-Newton Fluid Mech* 2016, **238**:92–99.

60. Luo R, Chen Y, Lee S: **Particle-induced viscous fingering: review and outlook**. *Phys Rev Fluids* 2018, **3**:110502.

61. Chen Y, Luo R, Wang L, Lee S: **Self-similarity in particle accumulation on the advancing meniscus**. *J Fluid Mech* 2021, **925**:A10.

62. Thiévenaz V, Sauret A: **Pinch-off of viscoelastic particulate suspensions**. *Phys Rev Fluids* 2021, **6**:L062301.

63. ** Thiévenaz V, Rajesh S, Sauret A: **Droplet detachment and pinch-off of bidisperse particulate suspensions**. *Soft Matter* 2021, **17**:6202–6211.
Polydisperse suspensions are common in both natural and industrial processes, but studies on the topic are rare regarding liquid bridge stretching. This study allows to better understand the physics of polydisperse suspensions through the investigation of bidisperse suspensions, taking into account species volume fraction and particle sizes.

64. Faletra M, Marshall JS, Yang M, Li S: **Particle segregation in falling polydisperse suspension droplets**. *J Fluid Mech* 2015, **769**:79–102.

65. * Fukushima Y, Higo Y, Matsushima T, Otake Y: **Liquid bridge contribution to shear behavior of unsaturated soil: modeling and application to a micromechanics model**. *Acta Geotech* 2021, **16**:2693–2711.
Interesting paper which is aimed to model the rheology of the wet granular media accounting for the forces associated with the multiple liquid bridges connecting a given particle with the neighboring particles.

66. Roy S, Luding S, Weinhart T: **Liquid redistribution in sheared wet granular media**. *Phys Rev E* 2018, **98**:52906.

67. Moghadam A, Tafreshi HV: **On liquid bridge adhesion to fibrous surfaces under normal and shear forces**. *Colloids Surf A Physicochem Eng Asp* 2020, **589**:124473.

68. Furmidge C: **Studies at phase interfaces. I. The sliding of liquid drops on solid surfaces and a theory for spray retention**. *J Colloid Sci* 1962, **17**:309–324.

69. Extrand CW, Kumagai Y: **Liquid drops on an inclined plane: the relation between contact angles, drop shape, and retentive force**. *J Colloid Interface Sci* 1995, **170**:515–521.

70. Hinduja C, Laroche A, Shumaly S, Wang Y, Vollmer D, Butt HJ, *et al.*: **Scanning drop friction force microscopy**. *Langmuir* 2022, **38**:14635–14643.

71. Pilat D, Papadopoulos P, Schaffel D, Vollmer D, Berger R, Butt HJ: **Dynamic measurement of the force required to move a liquid drop on a solid surface**. *Langmuir* 2012, **28**: 16812–16820.

72. Suda H, Yamada S: **Force measurements for the movement of a water drop on a surface with a surface tension gradient**. *Langmuir* 2003, **19**:529–531.

73. Matilda B, Molpeceres D, Maja V, Heikki N, Hokkanen MJ, Ville J, *et al.*: **Water droplet friction and rolling dynamics on superhydrophobic surfaces**. *Commun Mater* 2020:1.

74. Daniel D, Timonen JV, Li R, Velling SJ, Aizenberg J: **Oleoplaning droplets on lubricated surfaces**. *Nat Phys* 2017, **13**: 1020–1025.

75. McHale G, Gao N, Wells GG, Barrio-Zhang H, Ledesma-Aguilar R: **Friction coefficients for droplets on solids: the liquid–solid Amontons' laws**. *Langmuir* 2022, **38**:4425–4433.

76. Gao N, Geyer F, Pilat DW, Wooh S, Vollmer D, Butt HJ, *et al.*: **How drops start sliding over solid surfaces**. *Nat Phys* 2018, **14**:191–196.

77. Saal A, Straub BB, Butt HJ, Berger R: **Pinning forces of sliding drops at defects**. *Europhys Lett* 2022, **139**:47001.

78. Joanny J, De Gennes PG: **A model for contact angle hysteresis**. *J Chem Phys* 1984, **81**:552–562.

79. Bormashenko E, Musin A, Zinigrad M: **Evaporation of droplets on strongly and weakly pinning surfaces and dynamics of the triple line**. *Colloids Surf A Physicochem Eng Asp* 2011, **385**:235–240.

80. Song Q, Liu K, Sun W, Chen R, Ji J, Jiao Y, *et al.*: **Lateral and normal capillary force evolution of a reciprocating liquid bridge**. *Langmuir* 2021, **37**:11737–11749.

81. Butler MD, Vella D: **Liquid bridge splitting enhances normal capillary adhesion and resistance to shear on rough surfaces**. *J Colloid Interface Sci* 2022, **607**:514–529.

82. Tadmor R, Bahadur P, Leh A, N'guessan HE, Jaini R, Dang L: **Measurement of lateral adhesion forces at the interface between a liquid drop and a substrate**. *Phys Rev Lett* 2009, **103**: 266101.

83. ** Kumar S: **Liquid transfer in printing processes: liquid bridges with moving contact lines**. *Annu Rev Fluid Mech* 2015, **47**: 67–94.
a detailed review of the dynamics of liquid bridges in relation to various printing processes.

84. Bodenstein C, Sauer HM, Fernandez F, Dörsam E, Warsitz E: **Assessing the quality of pad-printed images evaluating edge sharpness**. In *Advances in printing and media technology bd. XLV. Warsaw, Poland, Slovenia: 45th International Conference of Iarigai*, vol. 45. IARIGAI; 2018:98–107.

85. Kapur N, Abbott SJ, Dolden ED, Gaskell PH: **Predicting the behavior of screen printing**. *IEEE Trans Compon Packag Manuf Technol* 2013, **3**:508–515, https://doi.org/10.1109/TCPMT.2012.2228743.

86. Sauer HM, Roisman IV, Dörsam E, Tropea C: **Fast liquid sheet and filament dynamics in the fluid splitting process**. *Colloids Surf A* 2018, **557**:20–27, https://doi.org/10.1016/j.colsurfa.2018.05.101.

87. Rieckmann M, Brumm P, Sauer HM, Dörsam E, Kummer F: **Pressure and shear flow singularities: fluid splitting and printing nip hydrodynamics**. *Phys Fluids* 2023, **35**:32120, https://doi.org/10.1063/5.0139000.

88. ** Fardin MA, Hautefeuille M, Sharma V: **Spreading, pinching, and coalescence: the Ohnesorge units**. *Soft Matter* 2022, **18**: 3291–3303, https://doi.org/10.1039/D2SM00069E.
A detailed review on the major phenomena accompanied flows in liquid bridges of various geometries, configurations as well as rheological properties.

89. Saffman PG, Taylor GI: **The penetration of a fluid into a porous medium or Hele-Shaw cell containing a more viscous liquid**. *Proc R Soc Lond Ser A Math Phys Sci* 1958, **245**:312–329.

90. Schäfer J, Roisman IV, Sauer HM, Dörsam E: **Millisecond fluid pattern formation in the nip of a gravure printing machine**. *Colloids Surf A* 2019, **575**:222–229, https://doi.org/10.1016/j.colsurfa.2019.04.085.

91. Brumm P, Ciotta N, Sauer HM, Blaeser A, Dörsam E: **Deep learning study of induced stochastic pattern formation in the gravure printing fluid splitting process**. *J Coat Technol Res* 2023, **20**:51–72.

92. Brumm P, Sauer HM, Dörsam E: **Scaling behavior of pattern formation in the flexographic ink splitting process**. *Colloids Interfaces* 2019, **3**:37.

93. Wu JT, Carvalho MS, Kumar S: **Emptying of gravure cavities containing shear-thinning liquids**. *J Non-Newton Fluid Mech* 2019, **268**:46–55, https://doi.org/10.1016/j.jnnfm.2019.04.001.

94. Wu JT, Carvalho MS, Kumar S: **Effects of shear and extensional rheology on liquid transfer between two flat surfaces**. *J Non-Newton Fluid Mech* 2019, **274**:104173, https://doi.org/10.1016/j.jnnfm.2019.104173.

95. ** Carvalho MS, Scriven LE: **Three-dimensional stability analysis of free surface flows: application to forward deformable roll coating**. *J Comput Phys* 1999, **151**:534–562, https://doi.org/10.1006/jcph.1999.6195.
Provides important scaling for the liquid bridge size in application to roll coating.

96. Brunton SL, Proctor JL, Kutz JN: **Discovering governing equations from data by sparse identification of nonlinear dynamical systems**. *Proc Natl Acad Sci USA* 2016, **113**:3932–3937.

97. Brunton SL, Noack BR, Koumoutsakos P: **Machine learning for fluid mechanics**. *Annu Rev Fluid Mech* 2020, **52**:477–508.

98. Brunton SL, Kutz JN: *Data-driven science and engineering: machine learning, dynamical systems, and control*. Cambridge University Press; 2022.

99. Brumm P, Weber TE, Sauer HM, Dörsam E: **Ink splitting in gravure printing: localization of the transition from dots to fingers**. *J Print Media Technol Res* 2021, **10**:81–93, https://doi.org/10.14622/JPMTR-2016.

100. Kaptanoglu AA, de Silva BM, Fasel U, Kaheman K, Goldschmidt AJ, Callaham J, *et al.*: **PySINDy: a comprehensive Python package for robust sparse system identification**. *J Open Source Softw* 2022, **7**:3994, https://doi.org/10.21105/joss.03994.

101. Montanero JM, Ponce-Torres A: **Review on the dynamics of isothermal liquid bridges**. *Appl Mech Rev* 2019, **72**:10803, https://doi.org/10.1115/1.4044467.

102. Brumm P, Fritschen A, Doß L, Dörsam E, Blaeser A: **Fabrication of biomimetic networks using viscous fingering in flexographic printing**. *Biomed Mater* 2022, **17**:45012.